

Temperature dependence of single particle excitations in a $S = 1$ chain: exact diagonalization calculations compared to neutron scattering experiments

M. Kenzelmann and P. Santini

Oxford Physics, Clarendon Laboratory, Oxford OX1 3PU, United Kingdom

(November 13, 2018)

Exact diagonalization calculations of finite antiferromagnetic spin-1 Heisenberg chains at finite temperatures are presented and compared to a recent inelastic neutron scattering experiment for temperatures T up to 7.5 times the intrachain exchange constant J . The calculations show that the excitations at the antiferromagnetic point $q = 1$ and at $q = 0.5$ remain resonant up to at least $T = 2J$, confirming the recent experimental observation of resonant high-temperature domain wall excitations. The predicted first and second moments are in good agreement with experiment, except at temperatures where three-dimensional spin correlations are most important. The ratio of the structure factors at $q = 1$ and at $q = 0.5$ is well predicted for the paramagnetic infinite-temperature limit. For $T \leq 2J$, however, we found that the experimentally observed intensity is considerably less than predicted. This suggests that domain wall excitations on different chains interact up to temperatures of the order of the spin band width.

PACS numbers: 75.10.Jm, 75.40.Gb, 75.40.Mg

I. INTRODUCTION

The properties of antiferromagnetic spin-1 Heisenberg chains result from the presence of strong quantum fluctuations in the ground state, preventing magnetic order even at zero temperature where thermal fluctuations are absent. The ground state is a macroscopic quantum state, a non-magnetic spin singlet, where the spin correlation function falls off exponentially with increasing distance.¹ At zero temperature an antiferromagnetic spin-1 chain has a hidden long-ranged spin order^{2,3} which can carry long-lived spin-1 triplet excitations despite the absence of conventional magnetic long-range order. These excitations can be regarded as domain walls⁴ of the hidden spin order and they have a mass $\Delta = 0.41J$ (J is the exchange constant) which is generated by strong quantum fluctuations and is not a result of an anisotropy in the system.^{1,5,6} The excitation spectrum of an antiferromagnetic spin-1 Heisenberg chain is fundamentally different from the equivalent spin-1/2 chain whose excitations are gapless spin-1/2 particles.⁷

At finite temperature, temperature fluctuations disorder the hidden "quantum order" and this leads to a renormalization of the triplet excitations. For $T < \Delta$, the triplet excitations are well-defined and the spin-wave velocity is constant, but their mass - defined as the excitation energy at the antiferromagnetic point - increases.⁸ This upward renormalization of the excitation energy is well described by a low-energy field theory, the non-linear sigma model.^{9,8,10} For finite temperatures, the excitations acquire a finite life-time due to collisions with thermally excited particles and the temperature dependence of the decreasing life-time of the excitations is well described by a semi-classical model of gapped spin-1 particles with a relativistic dispersion.^{11,8,10}

For $T > \Delta$, there is a cross-over to a qualitatively different behavior. In this temperature range the excitations are resonant at least up to $T = 2.7J$,⁸ but the

excitation width is nearly as large as the excitation energy and the spin-wave velocity decreases with increasing temperature. These high-temperature excitations can be regarded as domain walls of a local hidden spin order^{12,10} which is the remainder of the hidden long-range order at $T = 0$ K. However, a quantitative theoretical understanding of the high-temperature spin dynamics is missing at present.

In the lack of reliable analytical methods for a quantitative calculation of dynamical properties at finite $T > \Delta$ we calculated the scattering function numerically by exact diagonalization (ED). We considered finite spin-1 chains with an antiferromagnetic Heisenberg exchange, described by the Hamiltonian

$$\mathcal{H} = J \sum_i \mathbf{S}_i \cdot \mathbf{S}_{i+1}, \quad (1)$$

and calculated the dynamic structure factor and frequency moments for temperatures up to $T = 7.5J$. The results of the calculations were then compared with the measured neutron scattering spectrum of the antiferromagnetic spin-1 Heisenberg chain compound CsNiCl_3 .

CsNiCl_3 crystallizes in a hexagonal crystal structure, D_{6h}^4 space group and is one of the best model systems for investigating antiferromagnetic spin-1 Heisenberg chains. The spin-1 components are carried by Ni^{+2} which interact via a super-exchange involving Cl^{-} -ions. The super-exchange interaction J along the c-axis is much stronger than the super-exchange interaction J' in the basal plane. Thus CsNiCl_3 approximates a system of weakly coupled spin-1 chains. The Hamiltonian can be written as

$$\begin{aligned} \mathcal{H}_{\text{CsNiCl}_3} = & J \sum_i \mathbf{S}_i \cdot \mathbf{S}_{i+1} \\ & + J' \sum_{\langle i,j \rangle} \mathbf{S}_i \cdot \mathbf{S}_j - D \sum_i (\mathbf{S}_i^z)^2, \end{aligned} \quad (2)$$

with $J = 2.28$ meV and $J' = 0.044$ meV.^{13,5,14} The

sum in the basal plane includes the interaction between nearest-neighbors $\langle i, j \rangle$ only. The single-ion crystal-field anisotropy $D = 4 \mu\text{eV}$ is small enough that the exchange interaction between the spins is isotropic in spin space. A detailed description of the neutron experiments has been presented elsewhere.^{8,10,15,16}

This paper is structured as follows: Section II introduces the numerical calculations, and shows that the excitations are resonant up to at least $T = 2J$. In Section III energy-integrated quantities of the dynamic structure factor are quantitatively compared with the experiment and effects of biquadratic and next-nearest neighbor interactions on the excitations are discussed. Section IV addresses the temperature dependence of the expectation value of the Hamiltonian and shows that there is excellent agreement between experiment and theory. Section V summarizes the results.

II. EXACT DIAGONALIZATION

The scattering function was obtained numerically by ED for single spin-1 chains of finite length through the following formulae:

$$S^{zz}(q, \omega) = \frac{1}{\pi} \frac{1}{1 - \exp(-\beta\omega)} \Im(\chi^{zz}(q, \omega)) \quad (3)$$

$$\Im(\chi^{zz}(q, \omega)) = \pi \sum_{i,j} |\langle i | S_z(q) | j \rangle|^2 (n_i - n_j) \delta(\omega - (\omega_j - \omega_i)) \quad (4)$$

$$S_z(q) = \frac{1}{\sqrt{N_s}} \sum_R S_z(R) e^{iqR}, \quad (5)$$

where $|i\rangle$ are the exact eigenstates of the Hamiltonian, with energy ω_i , and Boltzmann population factors n_i . N_s is the number of spins in the chain, and $S_z(R)$ is the operator for the z component of the spin at position R . q is the wave-vector along the chain.

The calculation of finite temperature properties requires knowledge of the full spectrum of the Hamiltonian so that only rather small sizes can be handled. We used a chain with $N_s = 8$ sites with periodic boundary conditions. The dimension of the Hilbert space is $3^{N_s} = 6561$. To reduce the numerical effort, we exploit the conservation of the z component of the total spin $S_z^{\text{tot}} = \sum_R S_z(R)$, which makes the Hamiltonian matrix block-diagonal in the basis of eigenstates of S_z^{tot} . Since the operator $S_z(q)$ commutes with S_z^{tot} , matrix elements in Eq. 4 are nonzero only if $|i\rangle$ and $|j\rangle$ have the same value of S_z^{tot} . Thus, once the partition function (entering n_i and n_j) has been determined, the contribution of each S_z^{tot} eigenspace to the scattering function can be calculated independently.

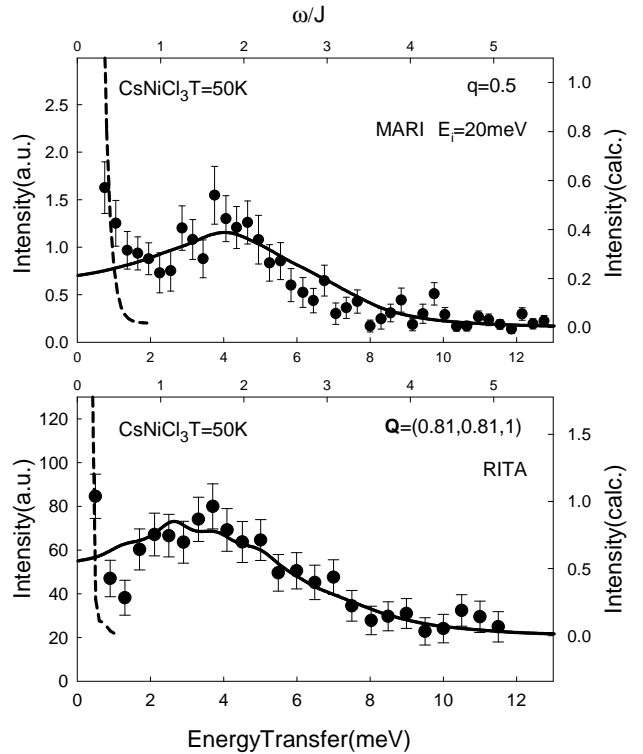


FIG. 1. The solid line represents the calculated dynamic structure factor $S^{zz}(q, \omega)$ for $q = 0.5$ (upper figure) and 1 (lower figure) at $T = 2J$ as a function of energy ω/J (top axes). The calculations for a finite chain of 8 sites were convoluted with a Lorentzian with a half width $0.3J$ in order to smooth out finite-size oscillations. The intensity is for a chain of $N_s = 8$ spins and such that $\sum_{k_i} \int d\omega S^{zz}(k_i, \omega) = \frac{S(S+1)N_s}{3}$ for $S = 1$ (right axes). The measured neutron scattering spectra are shown as solid circles and as a function of neutron energy transfer ω (bottom axes). The data were measured at $50 \text{ K} \simeq 2J$ using the RITA and the MARI spectrometer, taken from Refs.^{8,10}, and in units shown on the left axes. The axes on the left and right in the two figures were offset to account for the experimental background scattering. The dashed lines corresponds to the elastic scattering peak (not completely shown) which arises due to incoherent scattering at the sample and its environment.

Zero-temperature results have been obtained for sizes up to $N_s = 18$ by using the Lanczos algorithm to find the exact ground state of the system. In these calculations, the Hamiltonian matrix is further reduced to block-diagonal form by exploiting translational invariance, using a basis of states with given total wave-vector $K_{\text{tot}} = k_i = 0, 2\pi/N_s, \dots, 2\pi(N_s - 1)/N_s$. Then, $\langle i | S_z(q) | j \rangle \neq 0$ only if $S_z^{\text{tot}}(i) = S_z^{\text{tot}}(j)$ and $K_{\text{tot}}(i) = K_{\text{tot}}(j) + q$. The $T = 0$ dynamical structure factor can be obtained without performing an explicit calculation of all the spectrum of the Hamiltonian, by using in place of Eq. (1) a continued fraction representation of the dynamical susceptibility¹⁷, whose coefficients can be calculated recursively once the ground state is known. We

verified as a check of the calculations that the sum rule $\int d\omega S^{zz}(q, \omega) = \langle S_z(-q)S_z(q) \rangle$ is verified.

Fig. 1 shows the calculated $S^{zz}(q, \omega)$ as a function of energy transfer ω/J for $q = 0.5$ and $q = 1$ and for a temperature $T = 2J$. The energy spectra were obtained by convoluting the discrete spectra for finite chains with Lorentzian functions (width $0.3J$). q is given in units such that $q = 1$ corresponds to the antiferromagnetic point, which in theoretical work is often referred to as the π -point. Throughout the paper, the intensity of the calculated structure factor S^{zz} is given for a chain of N_s spins and normalized so that $\sum_{k_i} \int d\omega S^{zz}(k_i, \omega) = \frac{S(S+1)N_s}{3}$ because in an isotropic system one spin component carries exactly one third of the intensity.

The calculated excitation spectra are broad but still resonant at $T = 2J$, consistent with neutron scattering measurements which showed that the Haldane excitation survives as a resonant feature up to at least $T = 2.7J$.^{8,10} The calculated scattering weight at $q = 1$ is centered at $1.5J$ so that the scattering is at higher energies than at low temperature.⁸ At $q = 0.5$, the increase of the temperature has the opposite effect and the calculated scattering is centered clearly below the low-temperature maximum of the dispersion which is $\omega = 2.71J$.

The calculated excitation spectra are compared in Fig. 1 to neutron scattering data from CsNiCl_3 .^{8,10} The chains in CsNiCl_3 run along the c-axis, so the third component l of the wave-vector transfer $\mathbf{Q} = (h, k, l)$ corresponds to the wave-vector transfer along the chain. For the remainder of this paper q denotes both the wave-vector transfer along a single chain used in the theoretical calculations and the wave-vector transfer along the chain in CsNiCl_3 , thus $l = q$. The data in Fig. 1 was measured at $T = 50$ K which corresponds to $T = 2J$.

Three-dimensional (3D) spin-spin interactions - due to the interchain coupling J' - are most important for temperatures $T < 15$ K and they induce antiferromagnetic long-range order below $T_N = 4.84$ K.¹⁴ Above T_N , 3D interactions lead to a dispersion of the excitations perpendicular to the chain direction,¹⁴ which decreases with increasing temperature but 3D spin correlations may be still be important at $T = 50$ K. The measurements for $q = 1$ were performed at a wave-vector transfer $\mathbf{Q}_{1D} = (0.81, 0.81, 1)$ where the Fourier transform of the interchain coupling vanishes^{8,10} and where, within a Random Phase Approximation (RPA), the chains behave as if they were not coupled.^{5,6} So to first order the experiments probed the dynamics of isolated chains. For $q = 0.5$, the interchain coupling has only a negligible effect on the dynamic structure factor. Thus it is not important that the wave-vector transfer perpendicular to the chain varies in energy scans with the MARI spectrometer and the observed scattering for $q = 0.5$ can be directly compared to the calculations.

As shown in Fig. 1 the calculated and observed dynamic structure factor are in good agreement for $q = 0.5$ and $q = 1$ and the calculated excitation energies and

widths are well predicted by theory. The small differences between experiment and theory may arise from finite-size effects in the calculations.

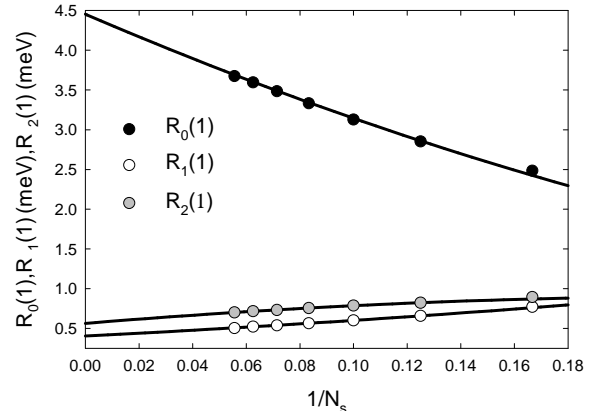


FIG. 2. $R_0(q) = S_{\omega>0}^{zz}(q)$, $R_1(q) = \langle \omega \rangle_{\omega>0}(q)$ and $R_2(q) = \sqrt{\langle \omega^2 \rangle_{\omega>0}(q)}$ for $q = 1$ obtained from ED calculations at zero temperature as a function of the inverse chain length $1/N_s$. The solid lines are fits to the data to extrapolate to an infinite chain as explained in the text.

The positive frequency moments of the spectrum are expected to be more reliable than the line-shape of $S^{zz}(q, \omega)$. For example, at $T = 0$ the ratio of the continuum to the Haldane mode contributions for a single chain is almost independent on the chain length and is well reproduced in small chain calculations, despite the fact that the line-shape of the continuum in $S^{zz}(q = 1, \omega)$ is not correct. The following moments were considered:

$$R_0(q) = S_{\omega>0}^{zz}(q) = \int_{\omega>0} S^{zz}(q, \omega) d\omega, \quad (6)$$

$$R_1(q) = \langle \omega \rangle_{\omega>0}(q) = S_{\omega>0}^{zz}(q)^{-1} \int_{\omega>0} \omega S^{zz}(q, \omega) d\omega, \quad (7)$$

$$R_2(q) = \sqrt{\langle \omega^2 \rangle_{\omega>0}(q)} = (S_{\omega>0}^{zz}(q)^{-1} \int_{\omega>0} \omega^2 S^{zz}(q, \omega) d\omega)^{1/2}. \quad (8)$$

For $k_B T \gtrsim 0.5J$ finite size effects in R_i appear to be small (this is seen by comparing results for $N_s = 4, 6, 8$). For smaller values of T , finite-size effects appear to be sizeable for $q = 1$ and very small for $q = 0.5$. We extracted the values of $R_i(q = 1)$ at $T = 0$ K for $N_s = \infty$ by performing a second-order finite-size scaling fit:

$$\tilde{R}_i(N_s) = R_i(N_s = \infty) + A_i/N_s + B_i/N_s^2. \quad (9)$$

A_i and B_i were calculated from R_i for $N_s = 14, 16, 18$. The extrapolated $\tilde{R}_i(N_s)$ were compared with the calculated $R_i(N_s)$ for $N_s = 6, 8, 10, 12$ and the results in Fig. 2 show that Eq. 9 holds down to rather small sizes, with just a small deviation for $R_0(q)(N_s = 6)$ (associated with a small $1/N_s^3$ correction).

III. QUANTITATIVE COMPARISON WITH EXPERIMENT

A. Excitations at $q = 0.5$

For $q = 0.5$, the coupling of the chains in CsNiCl_3 has a negligible effect on the dynamic structure factor and a direct comparison between the experiment and the ED calculations is possible. Fig. 3 shows the experimentally observed $R_0(q)$, $R_1(q)$ and $R_2(q)$ for $q = 0.5$ for temperatures between $T = 6$ and 200 K. The data were determined numerically from the neutron spectra measured using the MARI spectrometer after subtracting the flat background and accounting for the magnetic form factor of the neutron scattering intensity.¹⁰

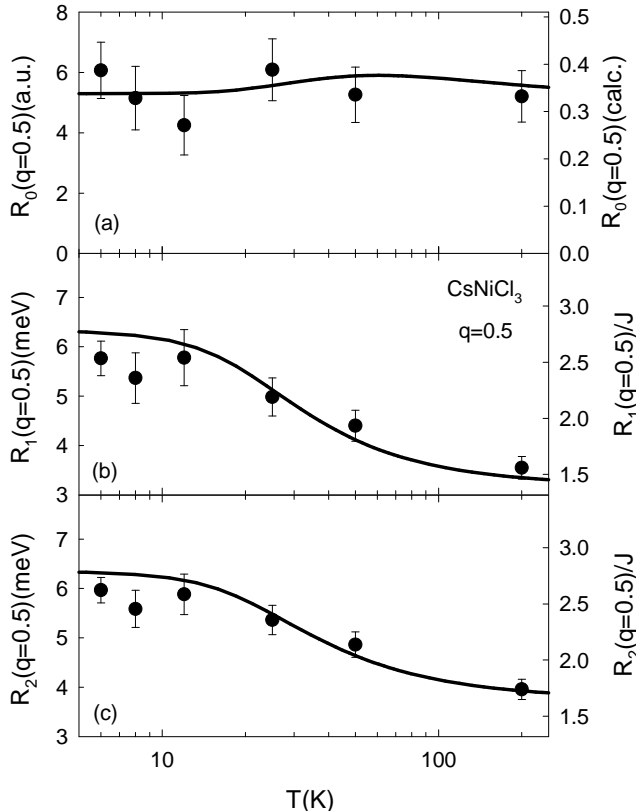


FIG. 3. (a) Integrated neutron scattering intensity $R_0(q)$ for positive energy transfers at $q = 0.5$ as a function of temperature on a semi-logarithmic plot. The data were measured using MARI and for temperatures between $T = 6$ and 200 K and taken from Ref.¹⁰. The intensity was determined by adding up the observed spectra for positive energy transfers after subtracting the flat background and accounting for the magnetic form factor.¹⁰ The solid line corresponds to the predicted $R_0(q = 0.5)$ obtained from ED calculations and fitted to the data, and it is shown in units shown of the right axis. (b) First energy moment $R_1(q = 0.5)$ of the neutron scattering spectra observed on the energy loss side. (c) Second energy moment $R_2(q = 0.5)$ of the scattering spectra on the energy loss side. Solid lines in (b-c) are ED predictions.

The ED results for $R_0(q = 0.5)$ were adjusted in a least-squares fit to the experimentally observed intensities using an overall scaling factor. No scaling factors were used for $R_1(q = 0.5)$ and $R_2(q = 0.5)$ which scale with the intrachain exchange $J = 2.28$ meV, accurately known from high-field magnetization measurements.¹³

The agreement between theory and experiment is excellent as shown in Fig. 3. The ED calculations reproduce the flat temperature dependence of the intensity at $q = 0.5$. A comparison with the overall scale is not possible because $S(\mathbf{Q}, \omega)$ was not measured in absolute units. Excellent quantitative agreement is found for the temperature dependence of the first and second moment at $q = 0.5$, as shown in Fig. 3(b)-(c). The small difference between the experiment and the calculations for $T < 10$ K, where $R_1(q = 0.5)$ and $R_2(q = 0.5)$ are slightly lower than predicted by our ED calculations, is at least partly due to finite-size effects: our ED calculations of finite chains overestimate the energy $\omega(q = 0.5) = 2.77J = 6.31$ meV, whereas a more accurate zero-temperature calculations give $\omega(q = 0.5) = 2.71J = 6.17$ meV.¹⁸

B. Excitations at $q = 1$

Fig. 4 shows $R_0(q)$, $R_1(q)$ and $R_2(q)$ for $q = 1$, measured between $T = 6$ and 70 K using the RITA spectrometer and compared to ED calculations of a finite chain of 8 sites. The neutron scattering measurements were performed at the non-interacting wave-vector \mathbf{Q}_{1D} ^{8,10} where the chains behave within RPA as if they were not coupled. To first order, the temperature dependence of $R_0(q = 1)$, $R_1(q = 1)$ and $R_2(q = 1)$ are thus expected to match that of a single chain.

$R_1(q = 1)$ is about $0.65J$ at zero temperature, and it is almost three times as large at $T = 2J$. This reflects the rapid increase of the excitation energy at $q = 1$ with increasing temperature.⁸ The zero-temperature value of $R_1(q = 1)$ is higher than the Haldane gap $0.41J$ due to the presence of a weak single-chain multi-particle continuum at higher energies.^{19,20} There is good agreement between the measured and calculated $R_1(q = 1)$ and $R_2(q = 1)$ for temperatures $T > 15$ K as shown in Fig. 4. Below this temperature, the experimentally observed $R_1(q = 1)$ and $R_2(q = 1)$ are consistently higher than predicted by the calculations. In this temperature regime, finite-size effects are important which make the calculated $R_1(q = 1)$ and $R_2(q = 1)$ (see Fig. 2) larger than those of an infinite chain and finite-size effects can thus not explain the difference between the experiment and the calculations.

The difference between the experiment and the ED calculations are probably due to interchain couplings, which are known to have a strong effect on the intensity of the excitations just above the ordering temperature, as shown in Fig. 5 of our experimental paper.¹⁰ Also, for temperatures $T < 12$ K a multi-particle continuum was

observed,^{15,16} which increases $R_1(q = 1)$ and $R_2(q = 1)$ due to the presence of scattering weight at high energy transfers.

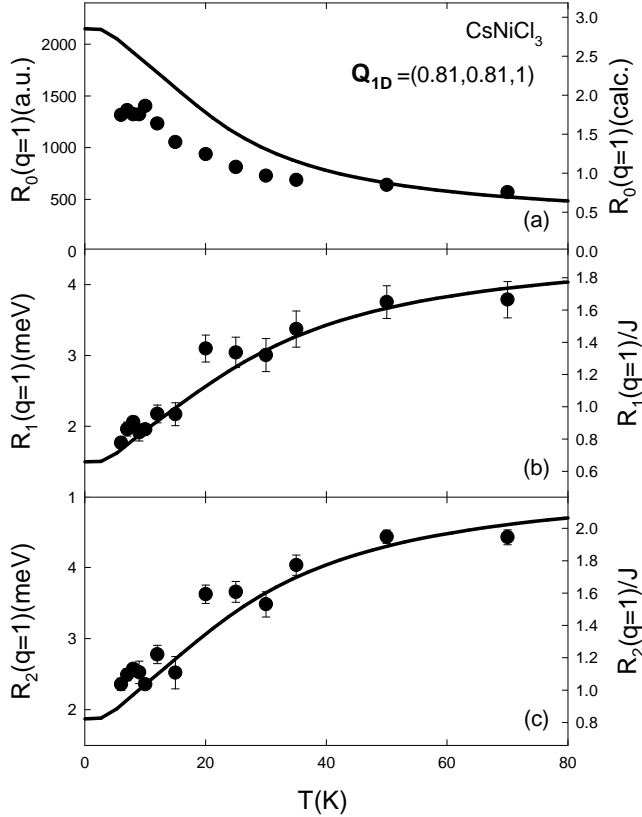


FIG. 4. (a) Integrated neutron scattering intensity $R_0(q = 1)$ observed at the non-interacting wave-vector $\mathbf{Q}_{1D} = (0.81, 0.81, 1)$ using the RITA spectrometer and taken from Ref.¹⁰. The solid line corresponds to the calculated $R_0(q = 1)$ obtained by ED calculations. The prediction was scaled to match the intensity at $T = 70$ K and is shown in units shown on the right axis. The error bars are smaller than the symbol size. (b-c) First and second energy moment $R_1(q = 1)$ and $R_2(q = 1)$ for the energy loss neutron scattering spectrum observed at \mathbf{Q}_{1D} using the RITA spectrometer. The solid line was obtained by ED calculations and the temperature and energy scaling was done using the intra-chain exchange $J = 2.28$ meV known from high-field magnetization measurements.

Figs. 4(a) and 5 show the experimentally observed $R_0(q)$ at $q = 1$ as a function of temperature. The data were measured using the RITA triple-axis and the MARI time-of-flight spectrometer, respectively.^{8,10} The ED calculations predict that at $T = 7.5J$ the ratio $R_0(q = 1)/R_0(q = 0.5)$ is equal to 1.26 and this can directly be tested with the neutron scattering experiments. At $T = 7.5J \simeq 200$ K the MARI measurements show that $R_0(q = 1)/R_0(q = 0.5) = 1.5(4)$, in good agreement with the calculations. At lower temperatures, however,

the experimentally observed $R_0(q = 1)/R_0(q = 0.5)$ is less than predicted and this is shown in Fig. 5. Since the temperature dependence of $R_0(q = 0.5)$ is in agreement with the calculations (Fig. 3), we conclude that the disagreement results from a reduced intensity $R_0(q)$ at the antiferromagnetic point $q = 1$. The disagreement is most pronounced for $T < 50$ K and may be due to the fact that the measurements were performed close to but not exactly at the non-interacting wave-vector \mathbf{Q}_{1D} .

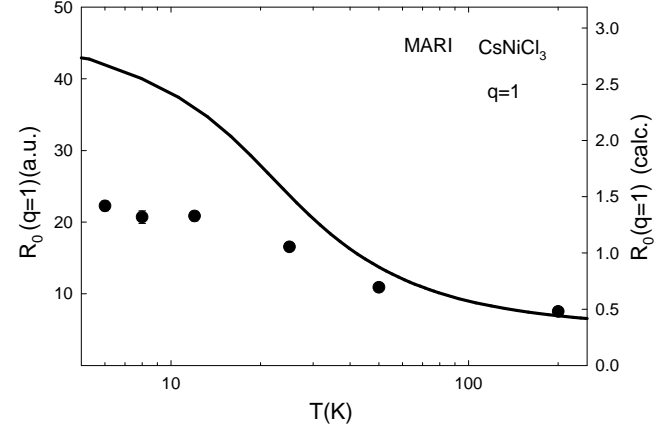


FIG. 5. Neutron scattering intensity at $q = 1$ observed using MARI for temperatures between $T = 6$ and 200 K as solid circles on a semi-logarithmic plot and taken from Ref.¹⁰. The intensity was determined by integrating the observed spectra for positive energy transfers after subtracting a flat background and correcting for the magnetic form factor.¹⁰ The solid line is the ED result for $R_0(q)$ at $q = 1$. The scaling was chosen to match the prediction $R_0(q = 1)/R_0(q = 0.5)$ and is thus in the same units as the scaling in Fig. 3.

Similar results were obtained, however, from an analysis of the RITA measurements which were performed *exactly* at the non-interacting 1D point \mathbf{Q}_{1D} in reciprocal space so that to first order the neutron spectrum should not be influenced by 3D interactions in the system. For the RITA measurements the scaling factor for $R_0(q = 1)$ can only be guessed because reliable measurements at $q = 0.5$ were not performed. Choosing the scaling factor such that the ED results match the observed $R_0(q = 1)$ at $T = 70$ K - which is known to be approximately true from the MARI measurements - the solid line shown in Fig. 4(a) is obtained. The discrepancy between the experiment and the numerical calculations is similar to that observed using the MARI spectrometer. At low temperatures there is a difference between theory and experiment of a factor of 1.6.

Finite-size effects may be important for $T < 15$ K, but these would underestimate the measured intensity rather than overestimate it (Fig. 2) and so they cannot explain the discrepancy between the experiment and the numerical calculations. This means the difference

between the experiment would be even bigger if longer chains had been considered in the calculations and the observed $R_0(q = 1)$ is *at least* a factor of 1.6 less than that calculated.

C. The influence of next-nearest neighbor, biquadratic and interchain spin-spin interactions

We examined the effect of next-nearest neighbor J_{nn} and biquadratic J_{biq} exchange interactions on the dynamic structure factor at zero temperature. The maximum in the dispersion $\omega(q = 0.5)$ was calculated numerically for a spin-1 Heisenberg chain with Hamiltonian \mathcal{H} (Eq. 1) and with additional terms

$$\mathcal{H}_{nn} = J_{nn} \sum_i \mathbf{S}_i \cdot \mathbf{S}_{i+2} \quad (10)$$

for next-nearest neighbor interactions or

$$\mathcal{H}_{biq} = J_{biq} \sum_i (\mathbf{S}_i \cdot \mathbf{S}_{i+1})^2 \quad (11)$$

for biquadratic spin interactions. The calculations were performed for chains with 12 sites. The calculated energies were then compared with the experimentally observed energies for $q = 0.5$ at low temperatures in order to estimate the strengths of next-nearest neighbor and biquadratic exchange interactions.

$\omega(q = 0.5)$ decreases for increasing J_{nn}/J and J_{biq}/J and increases when these exchange couplings are negative, as shown in Fig. 6(a). The measured values for $\omega(q = 0.5)$ are between 5.9 and 6.2 meV for various experiments with $6 \text{ K} < T < 12 \text{ K}$ (Ref.^{10,14,16}). This is consistent with $0 < J_{nn}/J, J_{biq}/J < 0.05$ and this range is shown in Fig. 6(a)-(c) as shaded area. The associated decrease in $R_0(q = 1)$ is at most a factor of 1.05 (Fig. 6(b)), which is much smaller than the observed reduction of $R_0(q = 1)$ by a factor of 1.6 at low temperatures. This shows that next-nearest neighbor and biquadratic exchange interactions cannot lead to the experimentally observed decrease in $R_0(q = 1)$.

Fig. 6(c) shows that the recently observed multi-particle continuum¹⁵ at high energy transfer carrying 12% of the total scattering at $q = 1$ cannot be caused by biquadratic or next-nearest neighbor interactions. This is because for $0 < J_{nn}/J, J_{biq}/J < 0.05$ the strength of the continuum is never more than 3% of the total scattering at $q = 1$. We note that our results for the valence bond solid model ($J_{biq}/J = 0.33$) are consistent with a previous study.¹⁸

At low temperatures $T < 12 \text{ K}$, the observed reduction of $R_0(q = 1)$ for \mathbf{Q}_{1D} is related to the correlation length ξ of the coherent state in the chains. It was shown that in CsNiCl_3 ξ is reduced from the value expected for single chains,¹⁰ which results in a wider peak of the structure factor $S(q)$ centered at $q = 1$. This means that $S(\mathbf{Q}_{1D})$

is reduced with respect to the value for uncoupled chains if the q -integrated intensity of $S(q)$ is to be unchanged.

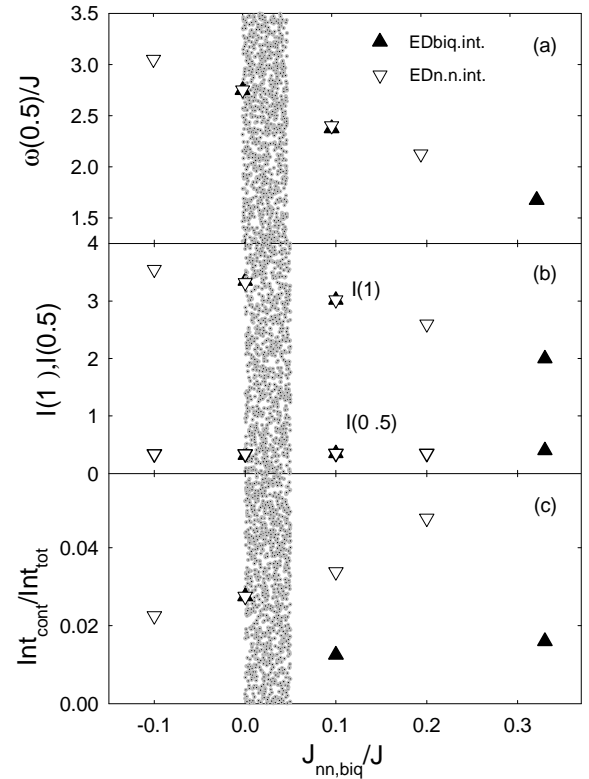


FIG. 6. (a) Zero-temperature ED results for the excitation energy at $q = 0.5$ as function of J_{nn}/J and J_{biq}/J . (b) ED results for the integrated intensity at $q = 1$ and at $q = 0.5$ at zero temperature as a function of J_{nn}/J and J_{biq}/J . (c) Zero-temperature results for the ratio of continuum intensity I_{cont} to total intensity I_{tot} at $q = 1$ as a function of J_{nn}/J and J_{biq}/J . The shaded area in (a)-(c) correspond to the possible J_{nn}/J and J_{biq}/J range for CsNiCl_3 .

The reduction of $R_0(q = 1)$ is also related to the multi-particle continuum at higher energies.^{15,16} The Hohenberg-Brinkman sum rule predicts that the first energy moment $F(q) = \int d\omega \omega S(q, \omega)$ of one-dimensional magnets with nearest-neighbor exchange interaction behaves as²¹

$$F(q) = -\frac{4}{3} \langle \mathcal{H} \rangle (1 - \cos(\pi q)). \quad (12)$$

It will be shown in the Appendix that this relation also holds for coupled chains with small interchain interactions. If the integrated intensity for a particular q is reduced, intensity necessarily has to be transferred to high energies so that the spectrum is consistent with the Hohenberg-Brinkman sum rule. This is because intensity at high energies contributes more to the first moment than scattering at low energies.

The comparison between the experiment and numerical calculations suggests that 3D correlations lower the

intensity at the non-interacting 1D point \mathbf{Q}_{1D} for $T < 2J$. Conservation of the total magnetic intensity then implies that this intensity is transferred to other parts of reciprocal space. The 3D dependence of the magnetic scattering suggests a coupling of domain walls on different chains for temperatures up to at least $T = 2J$. Further the coupling of the chains in antiferromagnetic spin-1 Heisenberg chains has a larger effect on the excitation spectrum and extends to higher temperatures than assumed so far. Possibly the hidden string order plays a decisive part in this effect because it allows the existence of spatially-extended coherent states to higher temperatures than would be possible in magnets without a similar spin string order.

IV. TEMPERATURE DEPENDENCE OF $\langle \mathcal{H} \rangle$

In our experimental paper¹⁰ the first energy moment sum rule was used to determine the temperature dependence of the expectation value of the Hamiltonian $\langle \mathcal{H} \rangle$ of a single spin-1 chain. Here we show that the first moment sum rule for single chains is also valid for weakly coupled chains. We also compare the experimentally determined values for $\langle \mathcal{H} \rangle$ to ED results.

The first energy moment of CsNiCl_3 based on the Hamiltonian given in Eq. 2 can be written as (see the Appendix)

$$F(\mathbf{Q}) = -4JF(1 - \cos(\mathbf{Q} \cdot \mathbf{c}/2)) \\ - 4J'F' \sum_j (1 - \cos(\mathbf{Q} \cdot \mathbf{a}_j)), \quad (13)$$

where \mathbf{a}_j are the lattice positions of the nearest neighbors and

$$F = F_\alpha = \sum_i \langle S_{\mathbf{r}_i}^\alpha S_{\mathbf{r}_i + \mathbf{c}/2}^\alpha \rangle, \\ F' = F'_\alpha = \sum_i \langle S_{\mathbf{r}_i}^\alpha S_{\mathbf{r}_i + \mathbf{a}_j}^\alpha \rangle,$$

for $\alpha = x, y, z$. The second term in Eq. 13 is always much smaller than the first term, mainly because $J' = 0.015J$, but also because $\text{Max}\{\sum_j (1 - \cos(\mathbf{Q} \cdot \mathbf{a}_j))\} = 4.5$ is only 2.25 times $\text{Max}\{(1 - \cos(\mathbf{Q} \cdot \mathbf{c}/2))\} = 2$. In addition, the wave-vector transfer in the experiments was mainly along the c -axis, which reduces the second term.

The dominant term in Eq. 13 is therefore

$$F(\mathbf{Q}) = -4JF(1 - \cos(\mathbf{Q} \cdot \mathbf{c}/2)) \\ = -4JF(1 - \cos(\pi q)), \quad (14)$$

which is directly proportional to $\langle \mathcal{H} \rangle = 3JF$ with \mathcal{H} given in Eq. 1. The expectation value of the Hamiltonian for a single chain can thus be obtained by fitting Eq. 14 to the q -dependence of the experimentally observed first energy moment $F(q)$.¹⁰

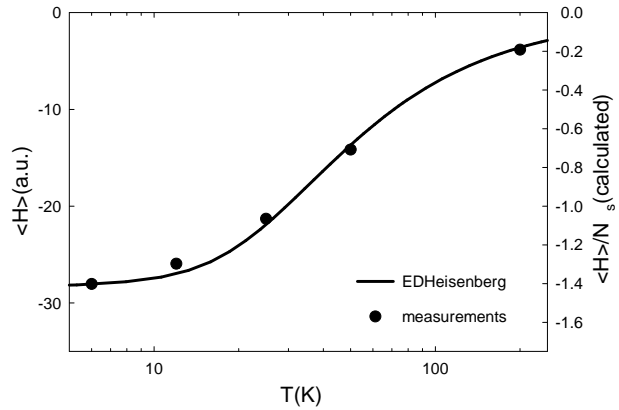


FIG. 7. The experimentally observed $\langle \mathcal{H} \rangle = J \sum_i \langle S_i S_{i+1} \rangle$ as solid circles and as a function of temperature on a semi-logarithmic plot and taken from Ref.¹⁰. $\langle \mathcal{H} \rangle$ was determined from the first energy moment measured at the different temperatures. The error bars are smaller than the symbol size. The solid line is the ED result for the temperature dependence of the mean energy per spin $\langle \mathcal{H} \rangle / N_s$.

Fig. 7 shows the experimentally determined $\langle \mathcal{H} \rangle$ from Ref.¹⁰, compared with our ED calculations. We find that there is excellent agreement between theory and experiment for the whole temperature range. A scaling factor was used to reach the agreement since $\langle \mathcal{H} \rangle$ was not measured in absolute units.

The calculated ground state energy per spin at zero temperature, $\langle \mathcal{H} \rangle / N_s = -1.41(1)J$, is consistent with a previous numerical study of much longer chains.³

V. CONCLUSIONS

We have performed exact diagonalization calculations of a finite antiferromagnetic spin-1 chain with 8 sites. The calculations confirm the recent experimental observation that the excitations are resonant for temperatures up to at least $T = 2J$. The temperature dependence of the calculated first and second energy moments for positive energy transfers is in good agreement with the measured neutron scattering¹⁰ except at low temperatures where spin correlations between chains are most important. Here the measured first and second moment for $q = 1$ are higher than predicted due to the presence of a multi-particle continuum at high energy transfers.

The measured intensity of the excitations at the non-interacting wave-vector is much weaker than that calculated for isolated chains, particularly for $T < 2J$. This suggests that solitons on different chains interact for temperatures up to at least $T = 2J$. The experimentally observed $\langle \mathcal{H} \rangle$ is in excellent agreement with exact diagonalization calculations for the entire temperature range considered in this study ($0.25J < T < 7.5J$).

APPENDIX

The first energy moment is defined as

$$F^{\alpha\alpha}(\mathbf{Q}) = \int_{\infty}^{\infty} \frac{d\omega}{2\pi} \omega S^{\alpha\alpha}(\mathbf{Q}, \omega) = -\frac{1}{2\hbar} < [\mathcal{H}, S_{\mathbf{Q}}^{\alpha}] , S_{-\mathbf{Q}}^{\alpha} >, \quad (15)$$

where the Fourier transform of the spin operators $S_{\mathbf{r}_i}^{\alpha}$ is defined as

$$S_{\mathbf{Q}}^{\alpha} = N_s^{-1/2} \sum_i \exp(-i\mathbf{Q}\mathbf{r}_i) S_{\mathbf{r}_i}^{\alpha}. \quad (16)$$

In the the case of CsNiCl_3 , the Hamiltonian includes both intrachain and interchain spin interaction, and it can be written as

$$\begin{aligned} \mathcal{H} = & \sum_{i,j} J_x S_{\mathbf{r}_i}^x S_{\mathbf{r}_i+\mathbf{c}/2}^x \\ & + J_y S_{\mathbf{r}_i}^y S_{\mathbf{r}_i+\mathbf{c}/2}^y + J_z S_{\mathbf{r}_i}^z S_{\mathbf{r}_i+\mathbf{c}/2}^z \\ & + J'_x S_{\mathbf{r}_i}^x S_{\mathbf{r}_i+\mathbf{a}_j}^x + J'_y S_{\mathbf{r}_i}^y S_{\mathbf{r}_i+\mathbf{a}_j}^y + J'_z S_{\mathbf{r}_i}^z S_{\mathbf{r}_i+\mathbf{a}_j}^z. \end{aligned} \quad (17)$$

In a cartesian coordinate system, the positions of the neighbors along the three directions in the basal plane are given as

$$\begin{aligned} \mathbf{a}_1 &= (a, 0, 0), \\ \mathbf{a}_2 &= (a/2, \sqrt{3}a/2, 0), \\ \mathbf{a}_3 &= (-a/2, \sqrt{3}a/2, 0). \end{aligned}$$

The first moment for $S^{xx}(\mathbf{Q}, \omega)$ can be split up into two terms, one containing the intrachain interactions J_{α} and the other the inter-chain interaction J'_{α} :

$$\begin{aligned} F^{xx}(\mathbf{Q}) = & -2J_y(F_y - F_z \cos(\mathbf{Q} \cdot \mathbf{c}/2)) \\ & - 2J_z(F_z - F_y \cos(\mathbf{Q} \cdot \mathbf{c}/2)) \\ & - \sum_j [2J'_y(F'_{y,j} - F'_{z,j} \cos(\mathbf{Q} \cdot \mathbf{a}_j)) \\ & + 2J'_z(F'_{z,j} - F'_{y,j} \cos(\mathbf{Q} \cdot \mathbf{a}_j))]. \end{aligned} \quad (18)$$

F_{α} and $F'_{\alpha,j}$ are the expectation values for spin-spin correlations along the chain direction and along either of the three direction in the basal plane:

$$F_{\alpha} = \sum_i < S_{\mathbf{r}_i}^{\alpha} S_{\mathbf{r}_i+\mathbf{c}/2}^{\alpha} >,$$

$$F'_{\alpha,j} = \sum_i < S_{\mathbf{r}_i}^{\alpha} S_{\mathbf{r}_i+\mathbf{a}_j}^{\alpha} >.$$

Due to the discrete rotational symmetry D_{6h}^4 in the magnetically disordered phase, spin correlations along all three equivalent direction in the basal plane are the same and

$$F'_{\alpha} = F'_{\alpha,j}, \quad j = 1, 2, 3.$$

For an isotropic spin chain $J_{\alpha} = J$, $F_{\alpha} = F$ and $F'_{\alpha} = F'$ for $\alpha = x, y, z$ and the first moment of $S(\mathbf{Q}, \omega)$ is

$$F(\mathbf{Q}) = -4JF(1 - \cos(\mathbf{Q} \cdot \mathbf{c}/2))$$

$$- 4J'F' \sum_j (1 - \cos(\mathbf{Q} \cdot \mathbf{a}_j)). \quad (19)$$

ACKNOWLEDGMENTS

We would like to thank Prof. R. A. Cowley and Dr. W. J. L. Buyers for enlightening discussions. The authors were supported by the Swiss National Science Foundation under Contract No. 83EU-053223 and No. 8220-053437, respectively.

- ¹ F. D. M. Haldane, Phys. Rev. Lett. **50**, 1153 (1983).
- ² M. den Nijs and K. Rommelse, Phys. Rev. B **40**, 4709 (1989).
- ³ S. R. White and D. A. Huse, Phys. Rev. B **48**, 3844 (1993).
- ⁴ G. Fáth and J. Sólyom, J. Phys.: Condens. Matter **5**, 8983 (1993).
- ⁵ W. J. L. Buyers, R. M. Morra, R. L. Armstrong, M. J. Hogan, P. Gerlach, and K. Hirakawa, Phys. Rev. Lett. **56**, 371 (1986).
- ⁶ M. P. Nightingale and H. W. J. Blöte, Phys. Rev. B **33**, 659 (1986).
- ⁷ D. A. Tennant, T. G. Perring, R. A. Cowley, and S. E. Nagler, Phys. Rev. Lett. **70**, 4003 (1993).
- ⁸ M. Kenzelmann, R. A. Cowley, W. J. L. Buyers, and D. F. McMorrow, Phys. Rev. B **63**, 134417 (2001).
- ⁹ T. Jolicœur and O. Golinelli, Phys. Rev. B **50**, 9265 (1994).
- ¹⁰ M. Kenzelmann, R. A. Cowley, W. J. L. Buyers, R. Coldea, M. Enderle, and D. F. McMorrow, cond-mat/0112188.
- ¹¹ K. Damle and S. Sachdev, Phys. Rev. B **57**, 8307 (1998).
- ¹² S. Yamamoto and S. Miyashita, Phys. Rev. B **48**, 9528 (1993).
- ¹³ A. A. Katori, Y. Ajiro, T. Asano, and T. Goto, J. Phys. Soc. Jpn. **64**, 3038 (1995).
- ¹⁴ R. M. Morra, W. J. L. Buyers, R. L. Armstrong, and K. Hirakawa, Phys. Rev. B **38**, 543 (1988).
- ¹⁵ M. Kenzelmann, R. A. Cowley, W. J. L. Buyers, R. Coldea, J. S. Gardner, M. Enderle, D. F. McMorrow, and S. M. Bennington, Phys. Rev. Lett. **87**, 017201 (2001).
- ¹⁶ M. Kenzelmann, R. A. Cowley, W. J. L. Buyers, Z. Tun, R. Coldea, and M. Enderle, cond-mat/0112152.

¹⁷ E. R. Gagliano and C. A. Balseiro, Phys. Rev. Lett. **59**, 2999 (1987).

¹⁸ M. Takahashi, Phys. Rev. B **50**, 3045 (1994).

¹⁹ M. D. P. Horton and I. Affleck, Phys. Rev. B **60**, 11891 (1999).

²⁰ F. H. L. Essler, Phys. Rev. B **62**, 3264 (2000).

²¹ P. C. Hohenberg and W. F. Brinkman, Phys. Rev. B **10**, 128 (1974).